

On the Repeated Use of Random FM Waveforms

Thomas J. Kramer, Matthew B. Heintzelman, Shannon D. Blunt
Radar Systems Lab (RSL), University of Kansas, Lawrence, KS

Abstract—Random frequency modulation (RFM) comprises a diverse class of noise radar waveforms that have been shown to possess a number of useful and practical attributes. Specifically, the inherent FM structure makes such waveforms amenable to high-power transmitters, while the high dimensionality arising from non-repetition facilitates the exploration of new operating modes. Of course, trade-offs in computational complexity and/or storage limitations may in some cases preclude the use of completely unique waveforms during a coherent processing interval (CPI). Consequently, here we examine the impact of the degree of repetition and the particular manner in which it occurs via examination of the point spread function, Monte Carlo simulation, and open-air experimental measurements.

Keywords—noise radar, waveform optimization, waveform diversity, moving target indication

I. INTRODUCTION

The origins of RFM waveforms (also referred to as FM noise) can be traced back to a US Navy patent filed in 1956 by Whiteley and Adrian that was issued in 1980 [1]. Since then, work on this class of noise waveform has continued to grow and expand (e.g. [2 - 4]), with the particular sub-class of RFM involving spectrum shaping (see [5] and references therein) enabling experimental demonstration of a variety of new capabilities, including real-time cognitive sense-and-notch operation [6], feasible complementary sidelobe cancellation [7], an intermodulation form of nonlinear radar [8], and more.

The spectrally-shaped FM nature provides the useful waveform properties of constant envelope and sufficient spectral containment, the combination of which limits the distortion incurred by high-power radar transmitters while adhering to mandated spectral emission masks [9]. This physically realizable structure permits the practical deployment of these high-dimensional, diverse waveforms and thereby supports the feasible development of new sensing modes. A key component in this context is the noise-like attribute of waveform uniqueness realized by non-repetition, while the pulse-to-pulse spectral density is effectively preserved to maintain coherency. Put another way, the unique pulse compression response for each RFM waveform yields a coherent mainlobe but independent sidelobes, introducing a range sidelobe modulation (RSM) effect [5], thereby resulting in incoherent averaging that reduces sidelobes by an additional factor of M (for M unique pulsed waveforms) when slow-time processing is performed.

This sub-class of spectrally-shaped RFM waveforms can be further delineated according to the particular design/implementation strategies employed, which themselves can be categorized according to whether or not per-waveform

optimization is necessary (see [5]). While RFM methods performing per-waveform spectrum-shaping optimization yield significantly lower range sidelobes than those that do not, they also incur a higher computational cost. One could conceivably perform this design process offline, though doing so may likewise involve a higher memory storage cost.

If and when these computational/memory limitations arise, prospective solutions could be to seek more efficient (or sub-optimal) per-waveform design approaches and/or exploit waveform representations that can be implemented using compact parameterizations (e.g. via the coded FM form in [10]). In the interest of more fully exploring the RFM implementation trade-space, here we instead approach the problem from the standpoint of determining the impact of permitting some degree of repetition to occur during the CPI, and subsequently consider appropriate strategies for doing so.

II. OVERVIEW OF RANDOM FM WAVEFORMS

The general and rather well-known form for an FM signal is

$$s(t) = \exp\left(j2\pi \int_{-\infty}^t f(\tau) d\tau\right) = \exp(j\theta(t)), \quad (1)$$

where $f(t)$ is the instantaneous frequency and $\theta(t)$ is the resulting instantaneous phase. The importance of this form lies in the obvious constant envelope it possesses and the somewhat less appreciated continuous phase that results from integrating frequency. The continuous phase aspect is needed to avoid the sinc-shaped “spectral skirt” [11] that occurs when phase discontinuities are present (e.g. for phase codes, see [10]).

The spectrally-shaped forms of RFM either impose further structure on (1) – these are the methods that are not per-pulse optimized [12, 13] – or take an iterative approach [7, 14-16] to impose a desired template onto the waveform’s spectral density

$$|S(f)|^2 = \mathbb{F}\{r(t)\}. \quad (2)$$

Here $r(t)$ is the autocorrelation of waveform $s(t)$ and $\mathbb{F}\{\bullet\}$ is the Fourier transform. Because these spectrum-shaping cost functions are highly non-convex, unique waveform initializations are effectively guaranteed to produce unique optimized waveforms via local minima solutions, thereby providing the requisite diversity. It is also worth noting that optimization of RFM waveforms without accounting for spectral shape (or at least out-of-band roll-off) tends to yield results with poor spectral containment (see [17]), which would incur greater transmitter distortion. Alternatively, even stricter containment also realizes a trade-off via the appearance of close-in “persistent” sidelobes that do not decrease with incoherent averaging during slow-time processing [18, 19].

In the context of repeating what are intended to be non-repeated waveforms, it is important to note that the slow-time combining of pulse-compressed responses from M independent RFM waveforms yields a $10 \log_{10}(M)$ sidelobe reduction. This effect occurs because the sidelobes are incoherent and therefore average in the same manner as noise. Consequently, repetition introduces redundancy and thus the degree of sidelobe suppression is degraded. That said, outside zero-Doppler the order of waveform repetition becomes important due to interaction with the slow-time combining, as discussed below.

III. ANALYSIS OF REPEATED RFM

While range-Doppler receive processing can be implemented in a variety of ways depending on the particular system/mode requirements, the general process involves pulse compression in fast-time (matched/mismatched filtering) followed by slow-time combining (Doppler/cross-range processing). For the purpose of discussion, discretize the m th waveform into N samples that adequately capture spectral roll-off, denoting the result as \mathbf{s}_m and the corresponding matched filter as \mathbf{h}_m . Likewise denote the collection of N discretized samples of the received echo response as $\mathbf{y}_m(\ell)$ relative to some range index ℓ . Then the matched filter response at range index ℓ is simply

$$x_m(\ell) = \mathbf{h}_m^H \mathbf{y}_m(\ell), \quad (3)$$

with $(\bullet)^H$ denoting the Hermitian operation.

Now collect the matched filter response over L range samples and across the M waveforms into the $M \times L$ matrix \mathbf{X} . Slow-time processing can then be realized by performing a Fourier transform on each $M \times 1$ column of \mathbf{X} , which can be simply written as

$$\mathbf{Z} = \mathbf{A}^H \mathbf{X} \quad (4)$$

with \mathbf{A}^H the discrete Fourier transform (DFT) matrix. For the purpose of Doppler visibility, we over-specify this matrix in terms of frequency granularity, resulting in \mathbf{A} having more columns than the M rows. It is also useful to express (4) for a single delay/Doppler sample via

$$z(\omega, \ell_o) = \mathbf{a}^H(\omega) \mathbf{x}(\ell_o), \quad (5)$$

where $\mathbf{a}(\omega)$ is an $M \times 1$ column of \mathbf{A} for slow-time Doppler frequency ω and $\mathbf{x}(\ell_o)$ is an $M \times 1$ column of \mathbf{X} at range index ℓ_o .

If we consider the special case of a single point scatterer without noise located at $(\omega=0, \ell_o)$ and employ the matched filter for each waveform, then \mathbf{Z} would contain the point-spread function (PSF), which is rather useful to assess the combined fast-time/slow-time response for a CPI of nonrepeating waveforms. For example, Fig. 1 illustrates the PSF for a single Pseudo-Random Optimized FM (PRO-FM) waveform [14] having a time-bandwidth product (TB) of 300 that is repeated over a CPI of $M = 500$ pulses. Aside from the particular range sidelobe response for this waveform, this PSF is essentially the same as one would obtain for any CPI of repeated waveforms, with the typical periodic sinc roll-off in Doppler (normalized

by pulse repetition frequency (PRF)) and likewise normalized by pulse width T in delay (only $\pm 10\%$ of delay is shown).

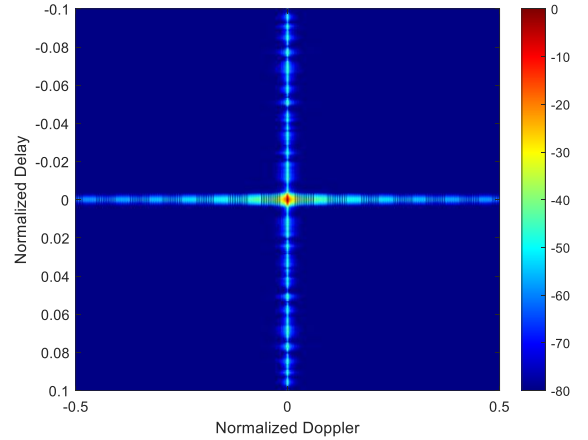


Fig. 1. Point-spread function for a CPI of $M = 500$ repeated PRO-FM waveforms

For this solitary scatterer case, the m th row of matrix \mathbf{X} contains the discretized autocorrelation \mathbf{r}_m for the m th waveform centered at ℓ_o . Consequently, the autocorrelation peak value in $\mathbf{x}(\ell_o)$ across the set of M waveforms remains phase coherent (for $\omega=0$ or arbitrary) and thus realizes a further coherent processing gain of M relative to noise when slow-time processing is performed. This result is the same regardless of whether or not the M waveforms are identical, unique, or somewhere in between.

However, the range sidelobes present in $\mathbf{x}(\ell < \ell_o)$ and $\mathbf{x}(\ell > \ell_o)$ do realize different outcomes from slow-time processing depending on the degree of waveform repetition. For a CPI of repeated waveforms, the autocorrelation is identical across the M pulses, and so the range sidelobes experience the same factor of M coherent integration gain as the mainlobe. At the other extreme, a CPI of completely unique waveforms means that each vector $\mathbf{x}(\ell < \ell_o)$ and $\mathbf{x}(\ell > \ell_o)$ contains M independent sidelobe values that are incoherent, therefore realizing an incoherent averaging effect the same as the noise. As a result, the sidelobes are also suppressed by a factor of M relative to the mainlobe when slow-time processing is performed [5], as illustrated in Fig. 2 for a CPI of $M = 500$ nonrepeating PRO-FM waveforms (note the prominent vertical response at zero Doppler from Fig. 1 has now disappeared).

Careful comparison of Figs. 1 and 2 also reveals that, while the zero-Doppler range sidelobes are suppressed in the latter, they also spread across Doppler to form a sidelobe pedestal instead of rolling off in the usual sinc manner for repeated waveforms. This effect is the range sidelobe modulation (RSM) phenomenon discussed in [5].

Between these two extremes lies the prospect of duplicating some of the waveforms. For the sake of illustration, consider partitioning of the M -pulse CPI into $N = M / K$ repeated sets of K unique waveforms (here M is evenly divisible by K , though this condition is not required in general). To further focus discussion, we assume each set of K unique waveforms occurs

in a contiguous block of pulses, though in practice any ordering is possible.

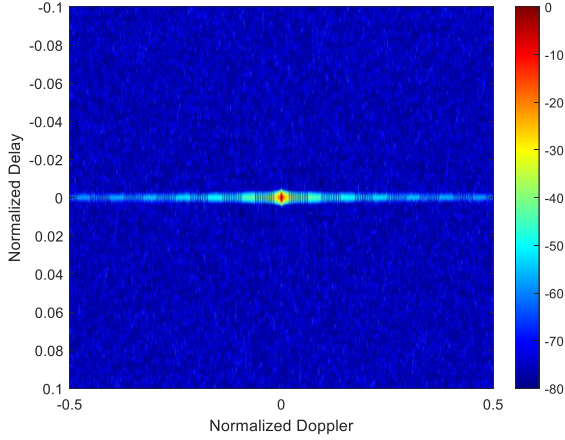


Fig. 2. Point-spread function for a CPI of $M = 500$ nonrepeating PRO-FM waveforms

To assess slow-time processing for this scenario it is useful to partition each Doppler steering vector from (4) and (5) as

$$\begin{aligned} \mathbf{a}(\omega) &= [1 \ e^{-j\omega} \ e^{-j2\omega} \ \dots \ e^{-j(M-1)\omega}]^T \\ &= [\bar{\mathbf{a}}_0^T(\omega) \ \bar{\mathbf{a}}_1^T(\omega) \ \dots \ \bar{\mathbf{a}}_{N-1}^T(\omega)]^T, \end{aligned} \quad (6)$$

where

$$\bar{\mathbf{a}}_n(\omega) = e^{-j(Kn)\omega} [1 \ e^{-j\omega} \ e^{-j2\omega} \ \dots \ e^{-j(K-1)\omega}]^T \quad (7)$$

for $n = 0, 1, \dots, N-1$. In other words, the steering vector partition $\bar{\mathbf{a}}_n(\omega)$ is the same for each value of n , aside from a scalar phase shift.

We can likewise partition the pulse-compressed responses in \mathbf{X} according to each block of K unique waveforms. Denote $\bar{\mathbf{x}}_n(\ell)$ for $\ell < \ell_o$ or $\ell > \ell_o$ as the corresponding n th partitioned set of responses within the interval of sidelobes. Therefore, (5) for $\ell \neq \ell_o$ could be written as

$$\begin{aligned} z(\omega, \ell) &= \mathbf{a}^H(\omega) \mathbf{x}(\ell) \\ &= \sum_{n=0}^{N-1} \bar{\mathbf{a}}_n^H(\omega) \bar{\mathbf{x}}_n(\ell) \\ &= \sum_{n=0}^{N-1} e^{-j(Kn)\omega} \bar{\mathbf{a}}_0^H(\omega) \bar{\mathbf{x}}_n(\ell) \end{aligned} \quad (8)$$

by invoking the invariant structure (aside from a scalar phase shift) of the partitioned steering vectors in (7).

The final line in (8) provides a convenient way to assess the impact of waveform ordering on sidelobe combining within each of the N waveform blocks. First, performing

$$\bar{\mathbf{a}}_0^H(\omega) \bar{\mathbf{x}}_n(\ell) \triangleq \rho_n(\omega, \ell) \quad (9)$$

realizes a factor of K sidelobe suppression due to incoherent averaging regardless of the relationship between waveform blocks. However, subsequent summation weighted by each $e^{-j(Kn)\omega}$ term in (8) is impacted by the relative waveform ordering across the blocks.

For instance, if waveform ordering is exactly the same across all N blocks then $\rho_n(\omega, \ell)$ for $n = 0, 1, \dots, N-1$ possesses coherency that translates into a factor of N gain in the form of a periodic sinc function. Of course, where the normal repeated waveform scenario involves a periodic sinc that repeats on $\pm\text{PRF}$ (or ± 1 if PRF-normalized), the extra factor of K in the exponential of (8) means that the periodic sinc in this case repeats on a Doppler interval of $\pm\text{PRF}/K$ (or $\pm 1/K$ if PRF-normalized). This effect is illustrated in Fig. 3 for $K = 10$ unique PRO-FM waveforms repeated in the same order for $N = 50$ times (so $KN = M = 500$ as before).

On the other hand, if the order of the K waveforms is randomized across the N blocks then two distinct conditions arise. For $\omega = 0$ the partitioned steering vector simplifies to $\bar{\mathbf{a}}_0(\omega = 0) = [1 \ 1 \ 1 \ \dots \ 1]^T$, meaning (9) becomes a summation of the sidelobes in $\bar{\mathbf{x}}_n(\ell)$ that is identical regardless of order across the N blocks. However, for $\omega \neq 0$ the resulting sequence of $\rho_n(\omega, \ell)$ values become incoherent when the waveform order is randomized, realizing a further factor of N sidelobe suppression from incoherent averaging. In other words, outside of $\omega = 0$ the randomized ordering of repeated waveform sets can achieve the same degree of sidelobe suppression as when all M waveforms are unique. Fig. 4 shows the PSF for this case using the same K and N as in Fig. 3.

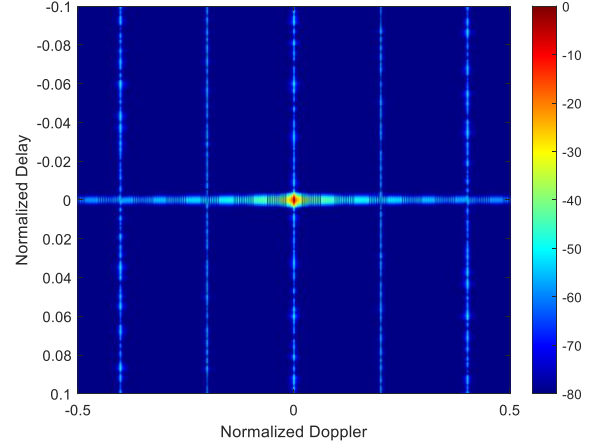


Fig. 3. Point-spread function for $K = 10$ nonrepeating PRO-FM waveforms, repeated identically $N = 50$ times (so $M = 500$)

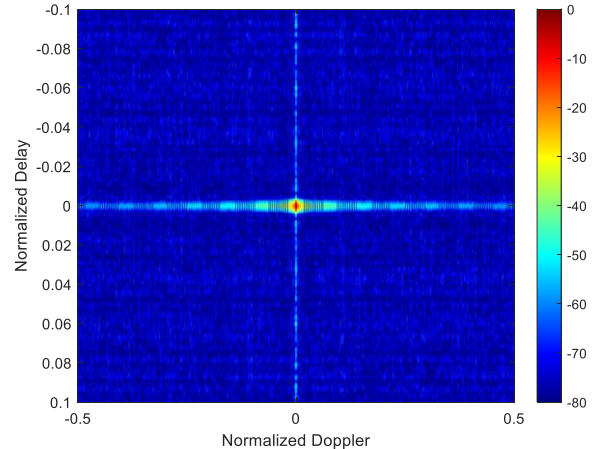


Fig. 4. Point-spread function for $K = 10$ nonrepeating PRO-FM waveforms randomly repeated $N = 50$ times (so $M = 500$)

Another way to assess behavior across these different waveform arrangements is through Monte Carlo simulation of sidelobe level. The notions of peak sidelobe level (PSL) and integrated sidelobe level (ISL) are more commonly used to evaluate performance of a given waveform in the range domain, though here we generalize them for use on the PSF.

Specifically, the number of unique waveforms within a CPI of 1000 pulses was varied from $K = 1$ to 600, and for each case 1000 independent trials were performed, with each trial involving an independent set of unique PRO-FM waveforms having $TB = 300$. Once each PSF is formed, the PSL and ISL values are determined both with and without the inclusion of zero-Doppler. In both cases, the zero-delay sinc rolloff in Doppler is excluded, since that portion of the delay/Doppler-normalized PSF is identical regardless of the waveform (for fixed TB). Note that PRO-FM is used here for convenience and these results are expected to generalize to other types of nonrepeating waveforms.

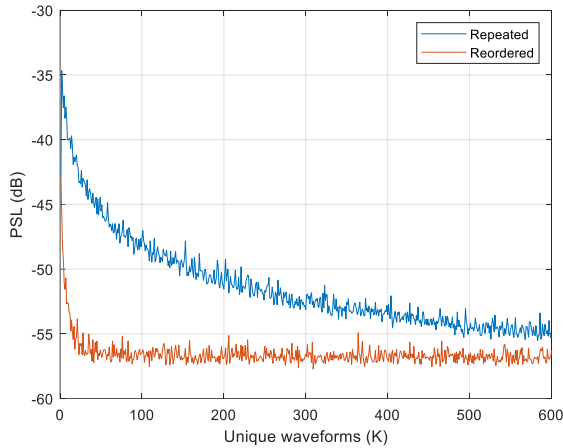


Fig. 5. Monte Carlo comparison of PSL (mean over 1000 trials) for repeated and randomly reordered sets of PRO-FM waveforms (excluding zero Doppler)

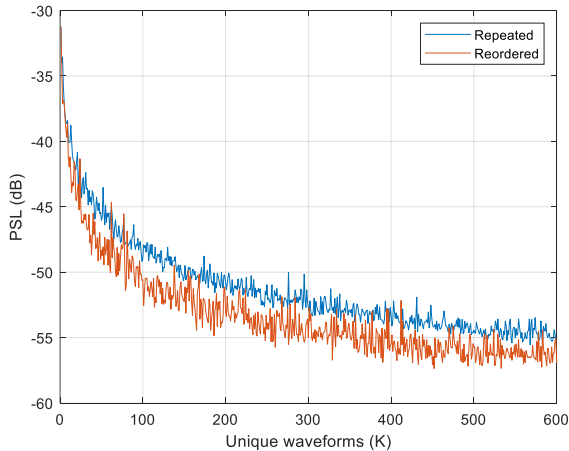


Fig. 6. Monte Carlo comparison of PSL (mean over 1000 trials) for repeated and randomly reordered sets of PRO-FM waveforms (including zero Doppler)

Fig. 5 shows the PSL after averaging across each set of 1000 trials for each number K of unique waveforms. We clearly

observe that randomizing the order of repeated waveforms essentially provides the same PSL (outside of zero-Doppler) regardless of the value of K (for $K > 1$). In contrast, the PSL realized for the repeated sets is capturing the repeated sinc peaks noted in Fig. 3 that decrease linearly with increasing K .

Fig. 6 also shows Monte Carlo PSL results, albeit with zero-Doppler (i.e. waveform autocorrelation) now included, which tends to dominate the PSL determination. Here we effectively see that the reordering of pulses has minimal PSL impact on the zero-Doppler component, with meaningful suppression requiring an increase in the number of unique waveforms K .

Interestingly enough, computing ISL (Fig. 7) reveals that overall sidelobe energy across the PSF is effectively conserved regardless of the number of unique waveforms or their ordering. The implication of this result (confirmed by observation) is that suppression of sinc peaks in Figs. 1 and 3 is offset by a higher background pedestal in Figs. 2 and 4, respectively.

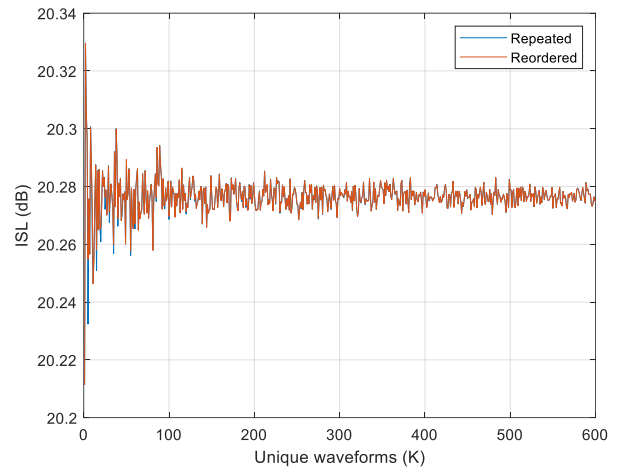


Fig. 7. Monte-Carlo comparison of ISL (mean over 1000 trials) for repeated and randomly reordered sets of PRO-FM waveforms (excluding zero Doppler)

IV. EXPERIMENTAL RESULTS

To verify these simulated results, free-space measurements were collected from the roof of Nichols Hall at the University of Kansas, illuminating moving vehicles traversing the intersection of 23rd and Iowa Streets about 1km away. Multiple trees and buildings were also within the field of view of the intersection. Three different CPIs were emitted, each composed of $M = 4,000$ pulses at a PRF of 50 kHz and a duty cycle of almost 12%.

The first and second CPIs were constructed from $K = 150$ unique PRO-FM waveforms having $TB = 300$, with the former using repeated sets and the latter using a random selection from the 150 possibilities for each pulse. In other words, this randomization is different from the random reordering into sets discussed above (used for explanation purposes), though the same behavior is expected. The third case then provides a performance baseline by allowing all $M = 4,000$ waveforms to be unique PRO-FM with the same $TB = 300$.

The received responses from the three cases were pulse compressed with the appropriate matched filter and then Doppler processed. Since the platform is stationary, simple

clutter cancellation using a projection at/around zero-Doppler was also performed.

Fig. 8 illustrates the baseline case using $M = 4,000$ unique PRO-FM waveforms, where we are focusing on the traffic intersection about 1 km away. The benefit of this multitude of unique waveforms is that range sidelobe modulation (RSM) is at/below the noise floor, and thus all movers are easily visible. The remaining cases were collected sequential to this one, so that the responses are readily comparable.

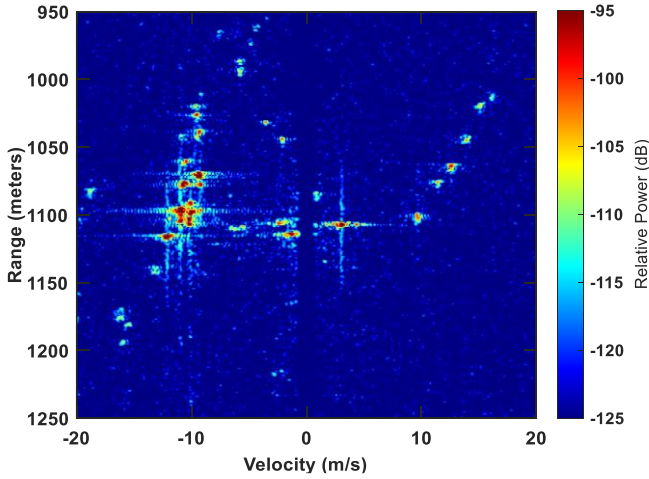


Fig. 8. Range-Doppler response for $M = 4,000$ unique PRO-FM waveforms after clutter cancellation

Figs. 9 and 10 then show the range-Doppler responses obtained from the repetition of $K = 150$ unique waveforms in the same order and via independent random selection, respectively. For the repeated case (Fig. 9) we observe the cohered sinc response that occurs at 8 m/s intervals in velocity (Doppler). In contrast, the random selection case (Fig. 10) appears to be nearly identical to the fully random case of Fig. 8, though a slightly higher background is discernible.

It is interesting to consider the trade-space that occurs when comparing the fully unique or randomized ordering cases observed in Figs. 8 and 10 against the repetition of a random set in Fig. 9. Because the latter preserves some coherence, even for sidelobes, there is ambiguity drawn into the repeated sinc responses that likewise lowers the RSM floor. Of course, portions of Doppler are also blocked by these additional sinc responses, which should not be confused with aliasing caused by Doppler frequencies exceeding $\pm PRF/2$. While one could certainly suppress some of these Doppler-localized responses in the same manner as clutter cancellation (e.g. see Fig. 11), the result effectively amounts to additional blind Dopplers. Therefore, the main take away is that repeated random waveforms introduces another trade-space depending on how the repetition occurs.

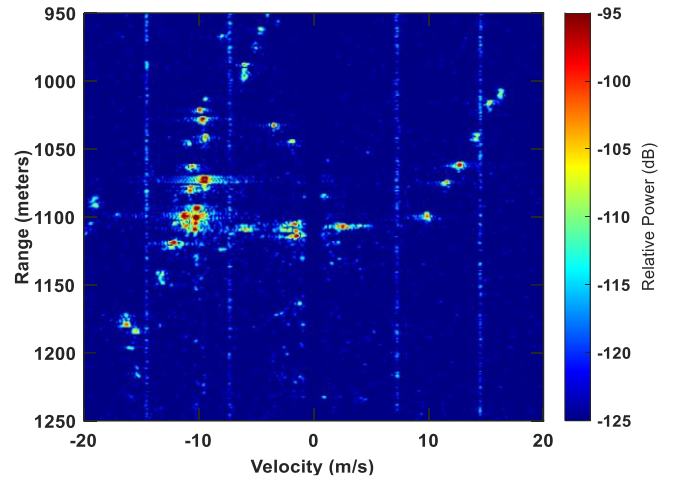


Fig. 9. Range-Doppler response for $M = 4,000$ pulses using repeated sets of $K = 150$ unique PRO-FM waveforms after clutter cancellation (zero Doppler suppression)

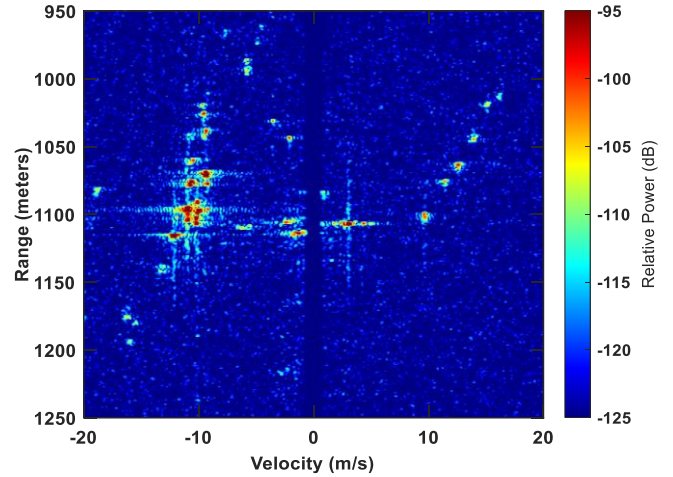


Fig. 10. Range-Doppler response for $M = 4,000$ pulses using random selection from $K = 150$ unique PRO-FM waveforms after clutter cancellation

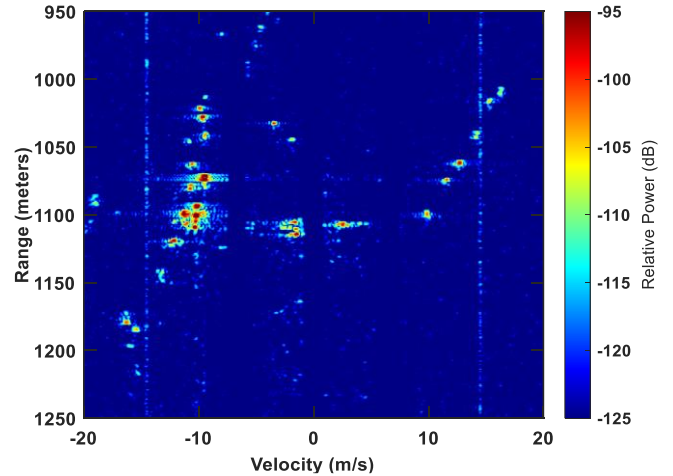


Fig. 11. Range-Doppler response for $M = 4,000$ pulses using repeated sets of $K = 150$ unique PRO-FM waveforms after clutter cancellation and first repeated sinc cancellation at $\pm PRF/K$

V. CONCLUSIONS

The nonrepeating nature of random FM waveforms has previously been shown to facilitate new radar capabilities that are amenable to high-power transmitters. Here we have explored the trade-space that arises when some degree of repetition is still permitted as a means to address possible limitations on processing/memory involved with the generation and storage of unique waveforms. It is observed that the repetition structure plays a significant role in the focusing or distribution of range sidelobe modulation (RSM) effects, which could be controlled based on the application.

REFERENCES

- [1] T.B. Whiteley, D.J. Adrian, "Random FM autocorrelation fuze system," U.S. Patent #4,220,952, issued 2 Sept. 1980, filed 17 Feb. 1956.
- [2] L. Guosui, G. Hong, Z. Xiaohua, S. Weimin, "The present and future of random signal radars," *IEEE Aerospace & Electronic Systems Mag.*, vol. 12, no. 10, pp. 35-40, Oct. 1997.
- [3] S.R.J. Axelsson, "Noise radar using random phase and frequency modulation," *IEEE Trans. Geoscience & Remote Sensing*, vol. 42, no. 11, pp. 2370-2384, Nov. 2004.
- [4] L. Pralon, B. Pompeo, J.M. Fortes, "Stochastic analysis of random frequency modulated waveforms for noise radar systems," *IEEE Trans. Aerospace & Electronic Systems*, vol. 51, no. 2, pp. 1447-1461, Apr. 2015.
- [5] S.D. Blunt, et al., "Principles & applications of random FM radar waveform design," *IEEE Aerospace & Electronic Systems Mag.*, vol. 35, no. 10, pp. 20-28, Oct. 2020.
- [6] B. Ravenscroft, J.W. Owen, J. Jakabosky, S.D. Blunt, A.F. Martone, K.D. Sherbondy, "Experimental demonstration and analysis of cognitive spectrum sensing & notching," *IET Radar, Sonar & Navigation*, vol. 12, no. 12, pp. 1466-1475, Dec. 2018.
- [7] C.C. Jones, C.A. Mohr, P.M. McCormick, S.D. Blunt, "Complementary frequency modulated radar waveforms and optimised receive processing," *IET Radar, Sonar & Navigation*, vol. 2021, no. 15, pp. 708-723, Apr. 2021.
- [8] J. Owen, S.D. Blunt, K. Gallagher, P. McCormick, C. Allen, K. Sherbondy, "Nonlinear radar via intermodulation of FM noise waveform pairs," *IEEE Radar Conf.*, Oklahoma City, OK, Apr. 2018.
- [9] *Manual of Regulations and Procedures for Federal Radio Frequency Management*, NTIA, Sept. 2017.
- [10] S.D. Blunt, M. Cook, J. Jakabosky, J. de Graaf, E. Perrins, "Polyphase-coded FM (PCFM) radar waveforms, part I: implementation," *IEEE Trans. Aerospace & Electronic Systems*, vol. 50, no. 3, pp. 2218-2229, July 2014.
- [11] N. Levanon, E. Mozeson, *Radar Signals*, Wiley-IEEE Press, 2004.
- [12] C.A. Mohr and S.D. Blunt, "Design and generation of stochastically defined, pulsed FM noise waveforms," *Intl. Radar Conf.*, Toulon, France, Sept. 2019.
- [13] E.R. Biehl, C.A. Mohr, B. Ravenscroft, S.D. Blunt, "Assessment of constant envelope OFDM as a class of random FM radar waveforms," *IEEE Radar Conf.*, Florence, Italy, Sept. 2020.
- [14] J. Jakabosky, S.D. Blunt, B. Himed, "Spectral-shape optimized FM noise radar for pulse agility," *IEEE Radar Conf.*, Philadelphia, PA, May 2016.
- [15] C.A. Mohr, P.M. McCormick, S.D. Blunt, C. Mott, "Spectrally-efficient FM noise radar waveforms optimized in the logarithmic domain," *IEEE Radar Conf.*, Oklahoma City, OK, Apr. 2018.
- [16] C.A. Mohr, S.D. Blunt, "FM noise waveforms optimized according to a temporal template error (TTE) metric," *IEEE Radar Conf.*, Boston, MA, Apr. 2019.
- [17] C.A. Mohr, P.M. McCormick, C.A. Topliff, S.D. Blunt, J.M. Baden, "Gradient-based optimization of PCFM radar waveforms," *IEEE Trans. Aerospace & Electronic Systems*, vol. 57, no. 2, pp. 935-956, Apr. 2021.
- [18] C.A. Mohr, S.D. Blunt, "Designing random FM radar waveforms with compact spectrum," *IEEE Intl. Conf. Acoustics, Speech & Signal Processing*, Toronto, Canada, June 2021.
- [19] M.B. Heintzelman, T.J. Kramer, S.D. Blunt, "Experimental evaluation of super-Gaussian-shaped random FM waveforms," *IEEE Radar Conf.*, New York City, NY, Mar. 2022.